JMEPEG
https://doi.org/10.1007/s11665-023-08793-6

1059-9495/$19.00

ORIGINAL RESEARCH ARTICLE

Ionic Copolymers Including Iodide and Dihydrogen Phosphate Anions for Increased Adsorption and Anticorrosion on Copper in Sulfuric Acid

Weiping Luo, Yueting Shi, Lingli Chen, Sijun Xu, Junle Xiong, Fang Gao, Hongru Li, and Shengtao Zhang

Submitted: 1 October 2022 / Revised: 22 April 2023 / Accepted: 17 September 2023

Two new ionic copolymers (poly(1,1′-(butane−1,4-diyl)bis(3-pentyl-1H-imidazol-3-ium)-bisiodide), ICP1, poly(1,1′-(butane−1,4-diyl)-bis(3-pentyl-1H-imidazol-3-ium)-bis(dihydrogen phosphate), ICP2) were synthesized by a simple ionic exchange method, which were characterized by the NMR spectra (^{1}H, ^{13}C and ^{31}P). The ICPs could be adsorbed on copper surface in mixed EtOH or MeOH/H_2SO_4 (0.01 mM solution) solvents (v/v, 1:1), and the ICPs-copper bonding was demonstrated by the ATR-IR (attenuated total reflectance-infrared spectroscopy), Raman, XPS (x-ray photoelectron spectroscopy) and XRD (x-ray diffraction), respectively. The electrochemistry analysis suggests that the ICPs adsorption films could prevent from copper corrosion in H_2SO_4 solution mainly through the cathode branch inhibition, and a remarkable anticorrosion efficiency of the ICPs of 0.010 g/L for copper in H_2SO_4 solution was obtained (97.19%) at 298 K. The peak corrosion inhibition efficiency of the ICPs for copper was found above 98% at 298 K (0.100 g/L). Furthermore, the contacting angles of the ICPs on copper surface were also measured and analyzed.

Keywords adsorption, anticorrosion, copper, counter anions, ionic copolymers

1. Introduction

Since copper and its alloys have excellent properties including fine conductivity of electricity and thermo and manufacturability, they are thus found in a variety of material and engineering fields (Ref 1-4). However, O_2, H_2O and CO_2 can yield serious rusts on copper surface, which restrain the application potentials of copper and its alloys (Ref 5, 6). Hence, sulfuric acid is often used to remove rusts on copper surface. On the other hand, copper may be corroded by acid pickling and cleaning (Ref 7, 8). Thus, it is significantly important to achieve efficient prevention of copper corrosion in sulfuric acid.

At the present time, organic corrosion inhibitor approach receives considerable interests to reach the above target, which provides a number of good properties such as easy performance, low cost, sustainability and no hurt to copper itself (Ref 9-13). Normally, such organic molecules may carry heterocycles or heteroatom functional groups or unsaturated covalent bonds (Ref 14-18). Hence, the lone pair electrons or delocalized electron cloudy inside these organic compounds can interact with the empty orbitals of copper. As a result, these compounds may be adsorbed on copper surface to form the adsorption films, which can restrain from the diffusion of corrosive ions and water molecules from the bulk solution to copper surface in acid medium.

Ionic molecules are competitive anticorrosion organic candidates due to a lot of unique characters such as amphiphilicity, non-volatility, non-flammability, fine thermal stability and non/low toxicity (Ref 19-23). It is known that ionic molecules such as imidazolium chloride and pyrrolidinium chloride are consist of cations and counter anions (Ref 24). Hence, it is thought that the molecular skeletons of ionic copolymers (ICPs) may carry huge heteroatoms and aromatic rings. Hence, the chemical chelation of ICPs with copper atoms can be reinforced (Ref 25, 26). This means that ICPs may process spontaneous adsorption on copper surface for highly efficient anticorrosion in H_2SO_4 medium.

Owing to huge challenges in the molecular design and chemical synthesis, few new ICPs including different counter ions were prepared for the protection of copper in acid medium. In this study, we propose to synthesize novel bisimidazolium-based amphiphilic ICPs including I^- and $H_2PO_4^-$ anions ((poly(1,1'-(butane−1,4-diyl)bis(3-pentyl-1H-imidazol-3-ium) bisiodide), ICP1, poly(1,1'-(butane−1,4-diyl)bis(3-pentyl-1H-

Weiping Luo and Yueting Shi contributed to this work equally and named as the co-first authors

Supplementary Information The online version contains supplementary material available at https://doi.org/10.1007/s11665-023-08793-6.

Weiping Luo, Lingli Chen, Sijun Xu, Fang Gao, Hongru Li, and **Shengtao Zhang**, College of Chemistry and Chemical Engineering, Chongqing University, Chongqing 400044, China; **Yueting Shi**, College of Chemistry and Chemical Engineering, Chongqing University, Chongqing 400044, China; and College of Chemistry and Environmental Engineering, Chongqing University of Arts and Sciences, Chongqing 400044, China; and **Junle Xiong**, Chongqing Kunding Environmental Protection Technology, Co. Ltd, Chongqing 400044, China. Contact e-mails: fgao@cqu.edu.cn, hrli@cqu.edu.cn, and stzhang@cqu.edu.cn.

Published online: 16 October 2023

imidazol-3-ium) bis(dihydrogenphosphate), ICP2)). Therefore, the target ICPs may undergo tough adsorption on copper surface, and thus the compact adsorption films can be formed on copper surface. It is thought that the large ionic radius and delocalized charge of I^- and $H_2PO_4^-$ can favor adsorption and anticorrosion of the ICPs on copper surface (Ref 27-30). As a consequence, copper may be well protected by the ICPs adsorption layers in H_2SO_4 solution. Thus, this study is trying to prepare new ionic copolymers to achieve strengthened adsorption and anticorrosion on copper in acid medium. The results presented in this work can guide us to develop ionic polymers for highly corrosion resistance on copper in acid medium.

2. Experimental

2.1 Materials and Characterizations

The synthesis routes of the target ICPs 1, 2 in this study were shown in Scheme 1. The starting compounds for the preparation of the ICPs were purchased from the Sigma-Aldrich Corporation. The organic solvents employed in this work were supplied by the Acros Chemical Corporation. The detail synthesis and characterization of the intermediate monomer IM and the target ICPs were presented in "Supplementary materials", including ^1H, ^{13}C and ^{31}P nuclear magnetic resonance (NMR) spectroscopy, elementary analysis and Fourier transform infrared spectroscopy (FT-IR).

The chemical structures of the monomer and target ICPs were characterized by various methods. The ^1H, ^{13}C and ^{31}P NMR spectra of the samples were determined with conventional methods at 298 K by using a Bruker nuclear magnetic resonance instrument. The ^1H (600 MHz), ^{13}C (150 MHZ) and ^{31}P NMR (600 MHz) peaks of the samples were calibrated by emplying tetramethylsilane as an internal reference. The Fourier transform infrared (FT-IR) spectra of the samples were determined with a Thermo Scientific Nicolet iS50 FT-IR spectrometer at 298 K. The Exeter ACE440 elemental analyzer was utilized to analyze and characterize the samples. The thermal stability of ICPs was measured with a Mettler Toledo TGA/DSC1/1600LF thermogravimetric synchronous thermal analyzer. A Waters gel permeation chromatography (GPC) system (HLC-8320 GPC) was employed to detect the molecular weights of the ICPs. The detail synthesis and characterization of the IM and ICPs were provided in "Supplementary Materials".

2.2 Copper Surface Characterization

The copper specimen was ground gradually with silicon carbide paper of different grits including 400#, 800#, 1200#, 2000#, 3000# and 5000#. Then, the ground metal sample was rinsed ultrasonically with ethanol and acetone, and dried under vacuum. And then, the copper sample was cleaned ultrasonically in nitric acid solution for a few seconds. Finally, the copper specimen was rinsed by deionized water and anhydrous ethanol, which was then dried under vacuum for the following determination.

The target ICPs were dissolved in mixed MeOH or EtOH/H_2SO_4 (0.01 mM solution) solvents (1:1, v/v), and the copper sample was immersed into the above solution at 298 K. The adsorption of the ICPs on copper surface reached the stable status after 8 h incubation. The copper surface adsorbed by the ICPs was characterized by various means at 298 K, which included the FT-IR (Fourier Transform Infrared spectroscopy), ATR-IR (attenuated total reflection infrared spectroscopy), Raman spectroscopy and XPS (x-ray photoelectron spectroscopy). The copper surface was further surveyed by the SEM (scanning electron microscopy) and AFM (atomic force microscopy).

A K-Alpha XPS Thermal Fisher (USA) instrument was used to determine the XPS of samples at 298 K. The aliphatic carbon C1S spectral line at 284.8 eV was used as the reference to caulcuate the energy. The surface morphology of the ICPs

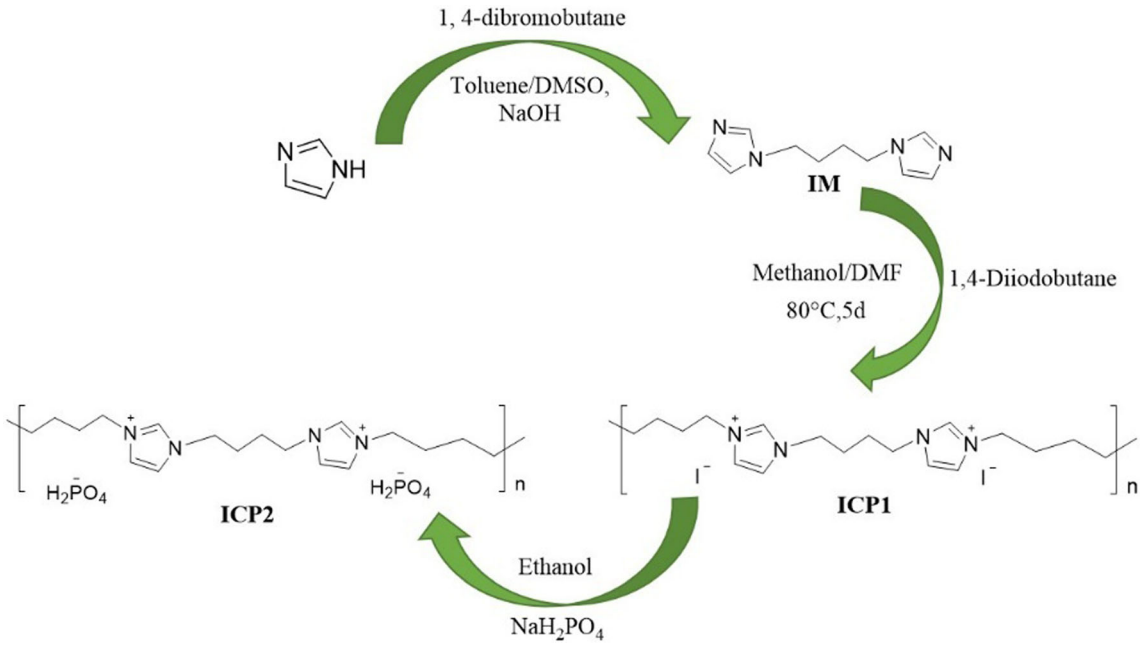

Scheme 1 Molecular structures and synthesis routes of the target ICPs

covered copper samples was analyzed by a scanning electron microscopy (SEM, Jeol JSM 3.5CF, Japan) and an atmoic formce microscopy (AFM, MFP 3D BIO, Asylum Research, USA), respectively.

A Nicolet iS50 apparatus supplied by the Thermal Fisher was used to collect the ex-situ FT-IR spectroscopy of the ICPs adsorbed copper samples, which were scanned in the range of 500-4000 cm^{-1}. The Raman spectroscopy of the ICPs covered Cu specimen was acquired by a Raman spectrometer (Renishaw, UK) at room temperature. A 514.5 nm argon ion laser beam at 1.7 mW was focused on the copper specimens. The Raman spectra were calibrated by the silicon line of 519 cm^{-1}. The contacting angle of copper sheet covered by the ICPs was measured by a contacting angle instrument (German Dataphysics). The detail experimental description of copper surface characterization was also found in the Supplementary Materials.

2.3 Electrochemistry Analysis

A three-electrode system was used for the electrochemical analysis, containing a WE, a RE (reference electrode) and a CE (counter electrode). In this study, a RE was a saturated calomel electrode (SCE) contained in a Luggin Capillary, while a CE was a platinum foil. The WE (working electrode) was made of the ground cylindrical copper sample with a diameter of 1.0 cm and a thickness of 0.2 cm. The copper electrode surface was mostly covered with epoxy resin. Therefore, the ICPs were adsorbed on the left blank part of copper electrode surface with a $0.25 \times \pi$ cm^2 area. Finally, the copper surface was cleaned with anhydrous ethanol and dried under vacuum.

An electrochemical workstation CHI660C of Chenhua (Shanghai) was used to obtain OCPs (open circuit potential) steady value of the WE within 30 min (Figure S1, Supplementary materials). The polarization curves of the WEs were recorded within $\pm$ 250 mV of the OCPs value at a 1.0 mV s^{-1} scanning rate. The electrochemical impedance spectroscopy (EIS) of the WEs was surveyed based on 5.0 mV amplitude of alternating voltage by varying the frequency from 100 to 0.01 Hz. All the electrochemical measurements were performed triply to guarantee the data reproducibility. The main electrochemical experiments were conducted at 298 K. In order to study the temperature influence on the anticorrosion of the ICPs on copper in sulfuric acid solution, the additional electrochemical experiments were also performed at 308 K and 318 K, respectively. It is noted that the samples were in the steady state when the impedance was measured by setting the stable open-circuit potential value parameters.

In this study, the corrosion inhibition efficiency (η) of the ICPs was calculated based on the Eq 1, 2 (Ref 31, 32),

$$\eta_j = \left(1 - \frac{j_{corr}}{j_{corr,0}} \times 100\%\right) \quad \text{(Eq 1)}$$

$$\eta_E = \frac{R_{ct} - R_{ct,0}}{R_{ct}} \times 100\% \quad \text{(Eq 2)}$$

where in, $j_{corr,0}$ and j_{corr} were corrosion current densities of the WEs unadsorbed and adsorbed by the ICPs, respectively, and $R_{ct,0}$ and R_{ct} showed charge transfer resistances of the WEs unadsorbed and adsorbed by the ICPs, respectively.

3. Results and Discussion

3.1 Synthesis and Characterization of the ICPs

The ICP2 was synthesized mildly, efficiently and shortly by a simple ionic exchange of the ICP1 that was prepared by the coplymerization between bisiodide and bisimidazolium. The obtained ICPs could be confirmed by the NMR spectra (^{1}H-, ^{13}C- and ^{31}P- NMR spectra) (Supplementary materials). It is shown that the ^{1}H-NMR chemical shifts of the ICPs were different from those of the intermediate monomer (IM). The results indicate that the polymerization could lead to a variation of deshielding magnetic field effect on the ^{1}H-NMR peaks. Furthermore, the number-average molecular mass (M_n) of the ICP1 and ICP2 were 1.051×10^4 (Da) and 1.038×10^4 (Da), respectively, and the weight-average molecular mass (M_w) of the ICP1 and ICP2 were 1.984×10^4 (Da) and 1.969×10^4 (Da), respectively. Hence, the low polydispersity (M_w/M_n, 1.9) suggests that the ICPs displayed a uniformity distribution. Besides, the lack of endothermic peaks in the differential scanning calorimeter (DSC) indicates that the ICPs were thermally stable (Figure S2, Supplementary materials) (Ref 33).

3.2 Adsorption of the ICPs on Copper Surface

3.2.1 SEM Micro Imaging. Although a number of light lines, channels, belts and marks produced by the sandpaper grinding were found on the freshly ground copper specimen surface, which was fairly clean and flat (Fig. 1a). However, the blank ground copper surface was severely corroded after 48 h immersion in acid solution, and the copper surface was totally destroyed and remarkably rough (Fig. 1b).

For contrast, the copper surface adsorbed by the ICPs was well protected after the corrosion in acid solution for 48 h (Fig. 1c, d, and e) and Fig. 2(a), (b), and (c), and the ground copper surface was even fully covered by the adsorption films of the ICPs. The results show that the ICPs could be adsorbed to copper surface, which might be well protected in H_2SO_4 solution. It is further found that the best adsorption layers of the ICPs on copper surface were obtained at 0.10 g/L.

3.2.2 AFM Micro Imaging. The AFM micro imaging was further employed to determine copper surface roughness (Fig. 3). The freshly ground copper showed a smooth surface with only a few nanometers of the average roughness (Ra, 4.462 nm). In contrast, the corroded blank copper surface was very rough (full of peaks and valleys) with a huge Ra of 41.782 nm after the immersion in H_2SO_4 medium for 8 h. While as compared to the corroded blank copper surface, the copper adsorbed by the ICPs displayed a flatter surface with the smaller Ra values of 10.084 nm (ICP1) and 9.021 nm (ICP2) after the incubation in 0.5 mol/L sulfuric acid solution.

The AFM micro imaging suggests that ICPs could be adsorbed on copper surface for yielding the good adsorption films, which showed super anticorrosion effect on copper surface in H_2SO_4 medium. In addition, the copper surface covered by the ICP2 was plainer than that adsorbed by the ICP1, indicating the better corrosion resistance nature of the ICP2.

3.2.3 Spectroscopy. *3.2.3.1 ATR-IR and Raman Spectroscopy.* The ICP2 exhibited two strong FT-IR signals including C = N (1646.46 cm^{-1}, 1557.75 cm^{-1}) and C-N (1441.55 cm^{-1}, 1158.06 cm^{-1}). While, the ATR-IR peaks of

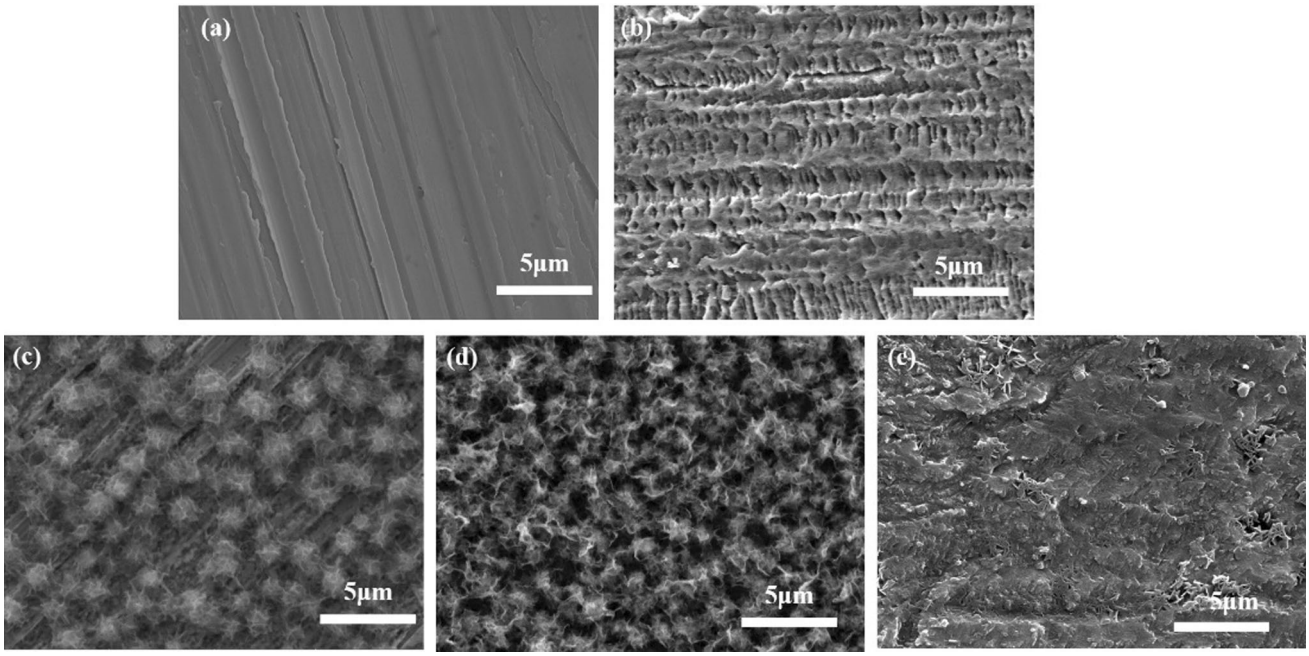

Fig. 1 SEM micrographs of copper surface after immersed in 0.5 mol/L H_2SO_4 solution for 48 h, (a) the freshly ground copper specimen, (b) the ground copper specimen after the immersion, (c-e) the ground copper specimen adsorbed by the ICP2 after the immersion (c) 0.01 g/L, (d) 0.10 g/L, (e) 0.20 g/L (the adsorption of ICP2 on copper surface: 8 h at 298 K)

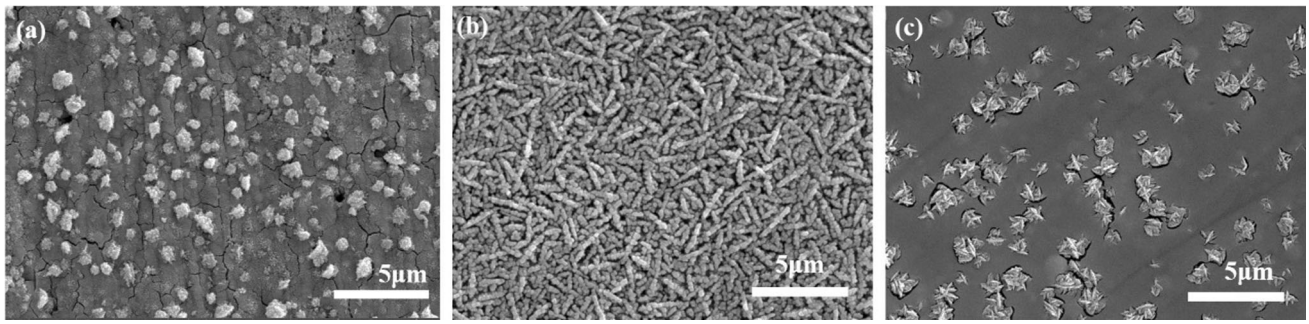

Fig. 2 SEM imaging micrographs of copper surfaces after immersed in 0.5 mol/L H_2SO_4 solution for 48 h, the ground copper specimen adsorbed by ICP1 of different concentrations, (a) 0.01 g/L, (b) 0.10 g/L, (c) 0.20 g/L. (the adsorption of ICP1 on copper surface: 8 h at 298 K)

the both bonds of the ICP2 adsorbed on copper surface showed a decrease (Fig. 4). Besides, the Raman spectral peak of N:Cu was found (Fig. 4) (Ref 34). In addition, the Raman peaks of C-N/C = N bonds in the ICP2 adsorbed on metal surface were also greatly reduced. It is also found that the ICP1 showed the similar FT-IR and ATR-IR spectroscopy to the ICP2 (Fig. 5). The results suggest that the ICPs were adsorbed on copper surface.

3.2.3.2 XPS. As compared to the corroded blank copper sample, the whole range XPS of the copper specimens adsorbed by the ICPs showed the enhanced C 1S peaks and the extra *N* 1 s, *I* 3d and *P* 2p after the immersion in surface acid (Fig. 6). However, the Cu(II) satellite peak in Cu 2P XPS was not found (Ref 35, 36). The results show that the ICPs adsorption films on copper surface could inhibit the oxidation of copper (I) to copper (II) in H_2SO_4 solution, thus they might well restrain the corrosion of copper in acid solution.

The Cu 2p, C 1 s, N 1 s, I 3d and P 2p XPS spectra of the ICPs covered copper samples after the incubation in sulfuric acid for 8 h were completely analyzed. The two asymmetric Cu $2p_{3/2}$ XPS peaks were found for the Cu-Bare sample (the corroded blank metal), which could be ascribed to Cu(0)/Cu(I) and Cu(II) (932.23 eV and 934.37 eV, Fig. 7, Table 1). But, the ICPs adsorbed copper samples displayed only a single and symmetric Cu $2p_{3/2}$ XPS peak after the soaking in sulfuric acid for 8 h, suggesting that Cu (II) was not yielded in acid solution. The results demonstrate that the adsorbed ICPs could prevent deep oxidation of copper (I) to Cu (II) in acid solution.

The three carbon states, including C-C (284.30 eV), C-O-C (284.80 eV) and O-C = O (288.01 eV), were confirmed in the C 1 s XPS of the corroded blank copper surface (Table 2) (Ref 37), which could be yielded by the carbon resources in air (Fig. 8). However, the ICPs covered copper surface showed the other two more states (C = N and C-N) (Fig. 8) after the incubation in sulfuric acid, which demonstrate that the ICPs were adsorbed on copper surface.

The three N states were identified by the *N* 1 s XPS of the ICPs adsorbed copper surface (Fig. 9). For example, the *C = N* (399.09 eV) and *C-N* (399.98 eV) were identified by the XPS of the copper surface adsorbed by the ICP1. In particular, the

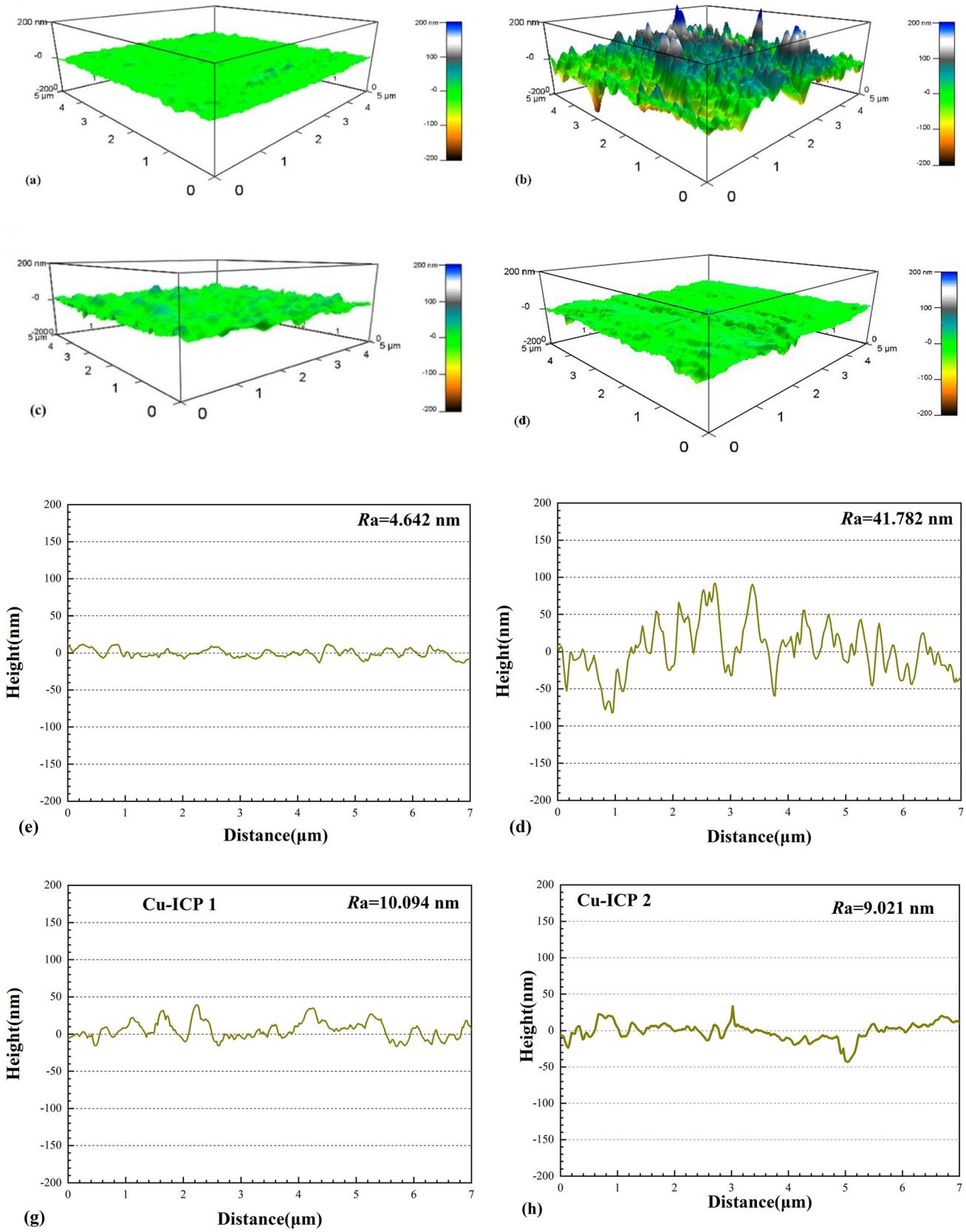

Fig. 3 AFM images of the copper surfaces after the immersion in acid medium for 8 h, (a) freshly ground copper surface, (b) the ground copper surface after the immersion, (c-d) the copper surface adsorbed by the ICPs after immersion, and (e-h) height images corresponding to (a-d) (the adsorption of ICPs of 0.10 g/L on copper surface: 8 h at 298 K)

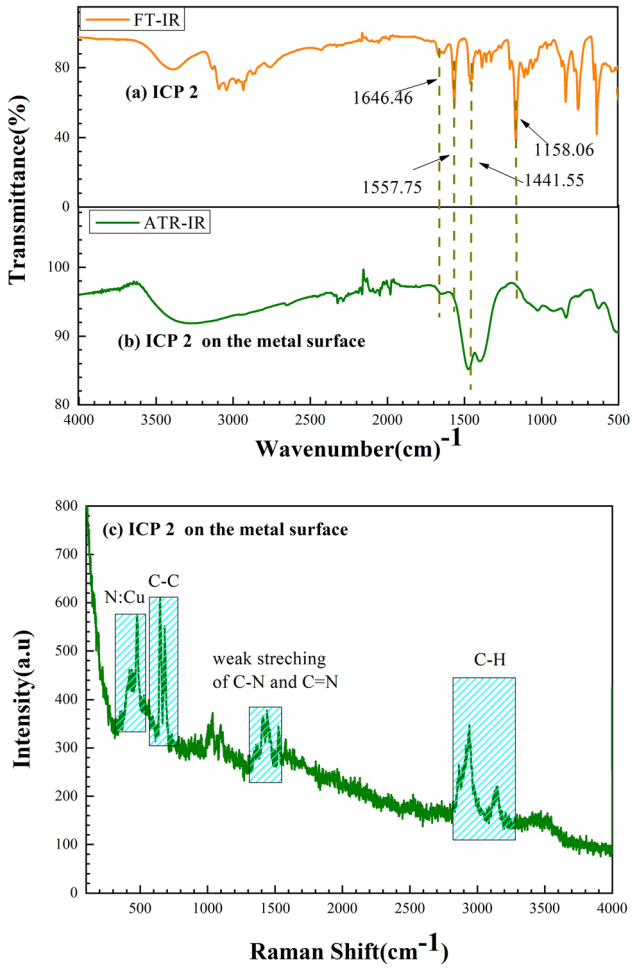

Fig. 4 (a) FT-IR spectra of ICP2, (b) FT-IR spectra of ICP2 adsorbed on Cu surface and (c) Raman spectra of ICP2 adsorbed on Cu surface (the adsorption of ICP2 of 0.10 g/L on copper surface: 8 h)

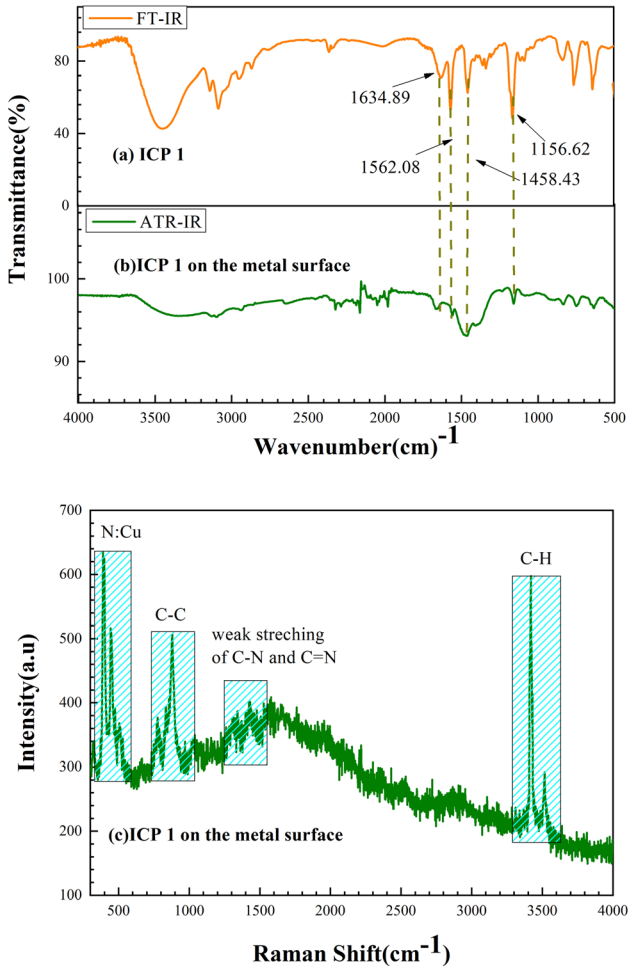

Fig. 5 (a) FT-IR spectra of ICP1, (b) ATR-IR spectra of the adsorbed ICP1 on Cu surfaces; and (c), Raman spectra of ICP1 adsorbed on Cu surface (the adsorption of ICP1 of 0.10 g/L on copper surface: 8 h at 298 K)

N:Cu could be verified (401.32 eV, Fig. 9, Table 3), which might be yielded by the chemistry coordination between the N-heterocycles in the ICPs and cuprous ions (Ref 38-40). Furthermore, the I 3d XPS displayed two peaks that were assigned to I^- (Figure S3, Table S1, Supplementary materials) (Ref 41). In addition, the peak at 133.17 eV in the P 2p XPS could be ascribed to $H_2PO_4^-$ (Figure S4, Table S2, Supplementary materials). In a word, the XPS of N 1 s, I 3d and P 2p suggest that the ICPs were adsorbed on copper surface to form adsorption films.

3.3 Electrochemistry Analysis

3.3.1 Polarization Curves. The Tafel diagrams of the WEs in sulfuric acid electrolyte were determined (Fig. 10). It is shown that the WEs adsorbed by the ICPs and the blank WE exhibited the similar curve, which suggests that the two electrodes could process a close electrochemical mechanism. It might consist of an oxidation reaction in the anode branch (electron losing) and a reduction reaction in the cathode branch (ORR, oxygen reduction, electron accepting).

It is shown that the Tafel curves in the anode and cathode branches showed a gradual movement towards the negative potential direaction with the increasing concentrations of the adsorbed ICPs. It is found that the movement was more significant in the cathode branch. Furthermore, the WEs adsorbed by the ICPs exhibited a decrease in the corrosion current density. Therefore, the Tafel plots demonstrate that the ICPs adsorption films could effectively prevent from copper corrosion in H_2SO_4 solution, which might be more remarkable in the cathode branch.

According to the Table 4, the electrochemical parameters including E_{corr} (corrosion potential), j_{corr} (corrosion current density), β_c (cathode Tafel slope), β_a (anode Tafel slope) and η_j (corrosion inhibition efficiency) were obtained. The data suggest that the polarization curves of the ICPs covered WEs shifted negatively towards the E_{corr}, indicating the copper electrode was protected by the adsorbed ICPs (Ref 42, 43).

The polarization plots show that the j_{corr} decreased gradually with the increase of the adsorbed ICPs' concentrations (from 0.01 to 0.10 g/L). The minimal value was yielded at 0.10 g/L (Table 4). Therefore, the ICPs reached the peak η_j value at 0.10 g/L (ICP1, 97.34%, and ICP2, 98.10%). The ICP2 had a larger η_j than the ICP1, which could be caused by the larger ionic radius and stronger charge delocalization of $H_2PO_4^-$ as compared with I^-. On the other hand, the η_j of the ICPs exhibited a decrease at the more concentrated solution (such as 0.20 g/L, ICP1, 94.34%, ICP2, 96.59%). This might be yielded

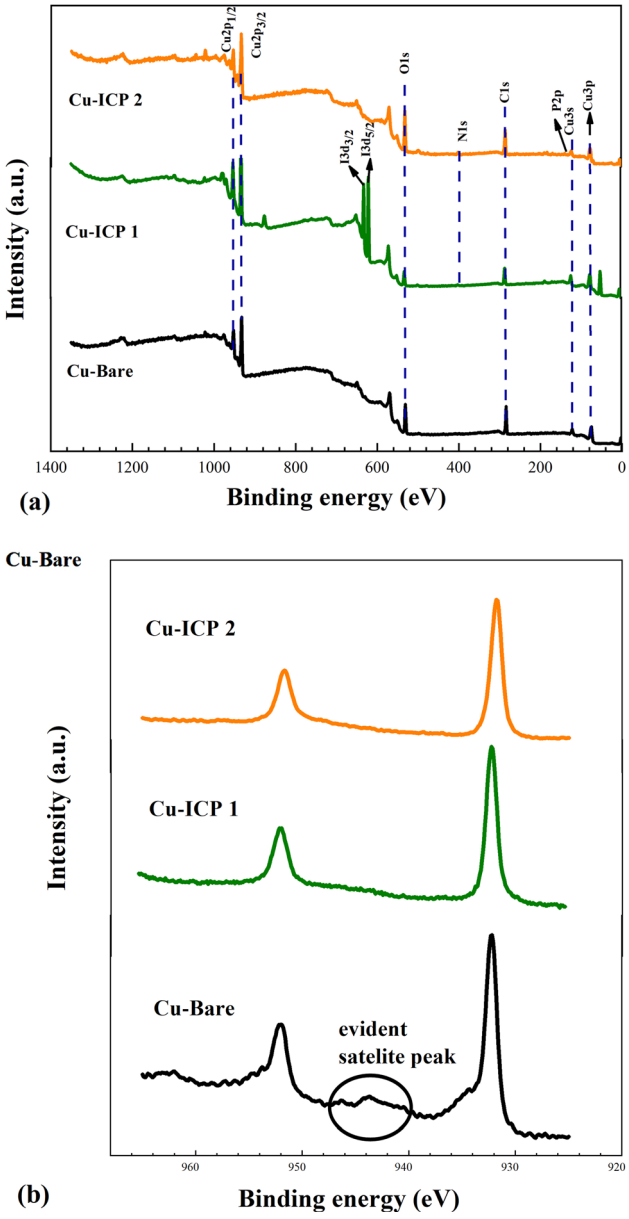

Fig. 6 (a) Whole range XPS of the blank Cu, the Cu samples covered by the stable ICPs, (b) Cu 2p XPS spectra of the blank Cu, and the Cu samples adsorbed by the stable ICPs after the incubation in sulfuric acid (the adsorption of ICPs of 0.10 g/L on copper surface: 8 h)

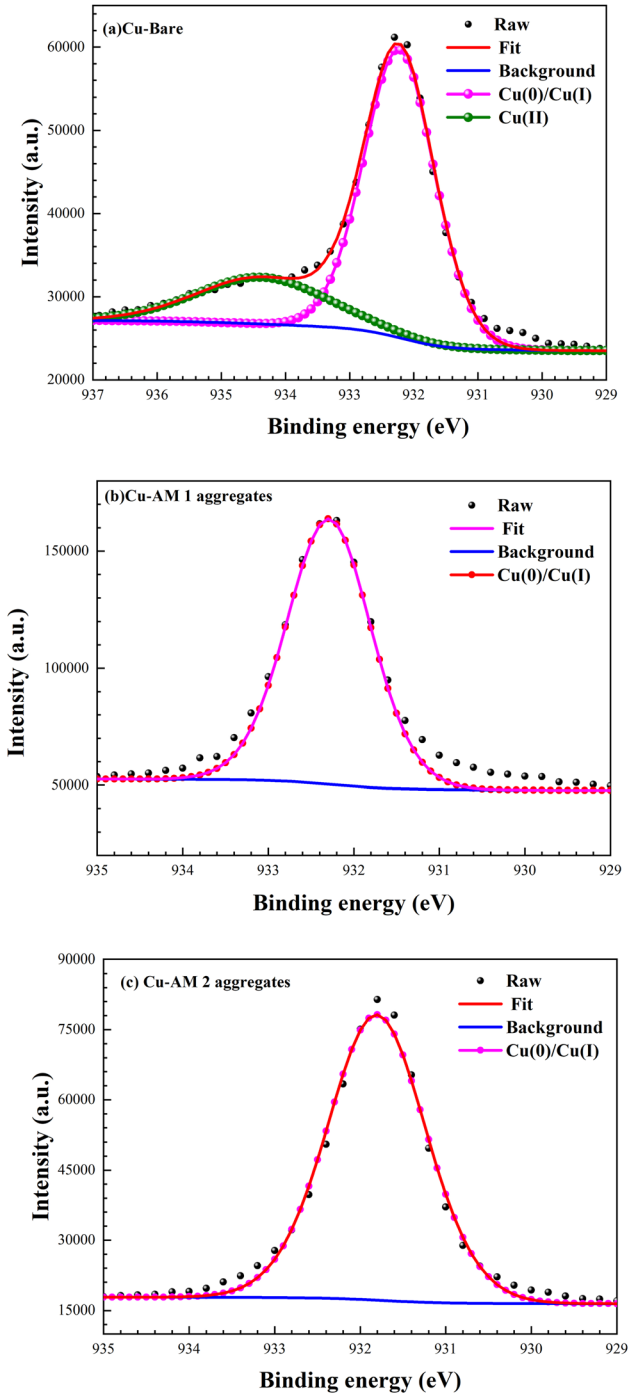

Fig. 7 Cu $2p_{3/2}$ XPS spectra of the studied copper surfaces, (a) the ground bare copper after included in blank 0.5 mol/L sulfuric acid solution, (b-c) the copper surface adsorbed by the ICPs after the immersion in 0.5 mol/L sulfuric acid solution (the adsorption of ICPs of 0.10 g/L on copper surface: 8 h at 298 K)

by the weaker adsorption and larger steric hindrance of the ICPs (Ref 44, 45). Overall, a large η_j of the ICP2 was achieved at 86.58% even at a very dilute solution (0.010 g/L). The polarization results reflect that the corrosion of copper in acid solution was inhibited by the ICPs.

In order to study the temperature influence on the anticorrosion of the ICPs for copper, the polarization curves of the adsorbed ICP2 (0.1 g/L) copper electrode in 0.5 M sulfuric acid solution under 308 and 318 K were measured, respectively. The polarization plots were given in Figure S5, and the electrochemical parameters acquired from the Tafel curves were listed in Table S3. It is found that with increasing the corrosion temperature, the j_{corr} showed a small enhancement, and the corrosion inhibition efficiency displayed a trivial decrease. In a word, the corrosion inhibition efficiencies of the ICP2 for copper in sulfuric acid were shown a slight decrease with

Table 1 De-convolution parameters of Cu $2p_{3/2}$ XPS spectra peaks obtained from the bare copper and the copper surface covered by the ICPs after the immersion in 0.5 M H_2SO_4 solution (the adsorption of ICPs of 0.10 g/L on copper surface: 8 h at 298 K)

Samples	Chemistry states	Binging energies, eV	FWHMs, eV
Cu-Bare	Cu(0)/Cu(I)	932.23	1.35
	Cu(II)	934.37	1.50
Cu-ICP 1	Cu(0)/Cu(I)	932.29	1.20
Cu-ICP 2	Cu(0)/Cu(I)	932.21	1.59

Table 2 De-convolution parameters of C 1 s XPS spectra peaks obtained from the bare copper and the copper surface adsorbed by the ICPs after the immersion in 0.5 M H_2SO_4 solution (the adsorption of ICPs of 0.10 g/L on copper surface: 8 h at 298 K)

Samples	Chemistry states	Binging energies, eV	FWHMs, eV
Cu-Bare	C-C	284.3	1.12
	C-O-C	284.8	1.29
	O-C=O	288.01	1.68
Cu-ICP 1	C-C/C-H	284.26	1.1
	C=N	284.8	1.24
	C-O-C	285.99	1.4
	C-N	287.49	0.62
	O-C=O	288.49	0.78
Cu-ICP 2	C-C/C-H	282.39	2.29
	C=N	284.33	1.19
	C-O-C	284.8	0.96
	C-N	285.61	2
	O-C=O	288.3	1.76

remarkably increasing the corrosion temperature in acid solution (298 K, 97.34%; 308 K, 96.28%, 318 K, 95.23%). The results indicate that the corrosion temperature was shown little effect on the anticorrosion of the ICPs for copper in H_2SO_4 medium, suggesting that the ICPs can form tight adsorption films on copper surface, and thus show extensive application potentials under different temperature.

3.3.2 Electrochemical Impedance Spectroscopy. The corrosion inhibition of the ICPs for copper in H_2SO_4 electrolyte was further determined by the electrochemical impendence spectroscopy (EIS). The Nyquist curves for the blank WE and the ICPs covered WEs are depicted in Fig. 11 and12.

It is found that blank WE displayed a little semicircle at high frequency and a line at low frequency (Ref 11, 46). It is accepted that the high frequency is related to charge transfer and double layer capacitance. And, the low frequency effect is caused by the Warburg impedance, which is yielded by the diffusion of the dissolved oxygen molecules in the bulk solution to copper electrode/bulk solution interface or the movement of copper ions from the copper surface to bulk acid medium.

It is observed that that ICPs adsorbed WEs showed decreased or even lost Warburg impedance in the Nyquist

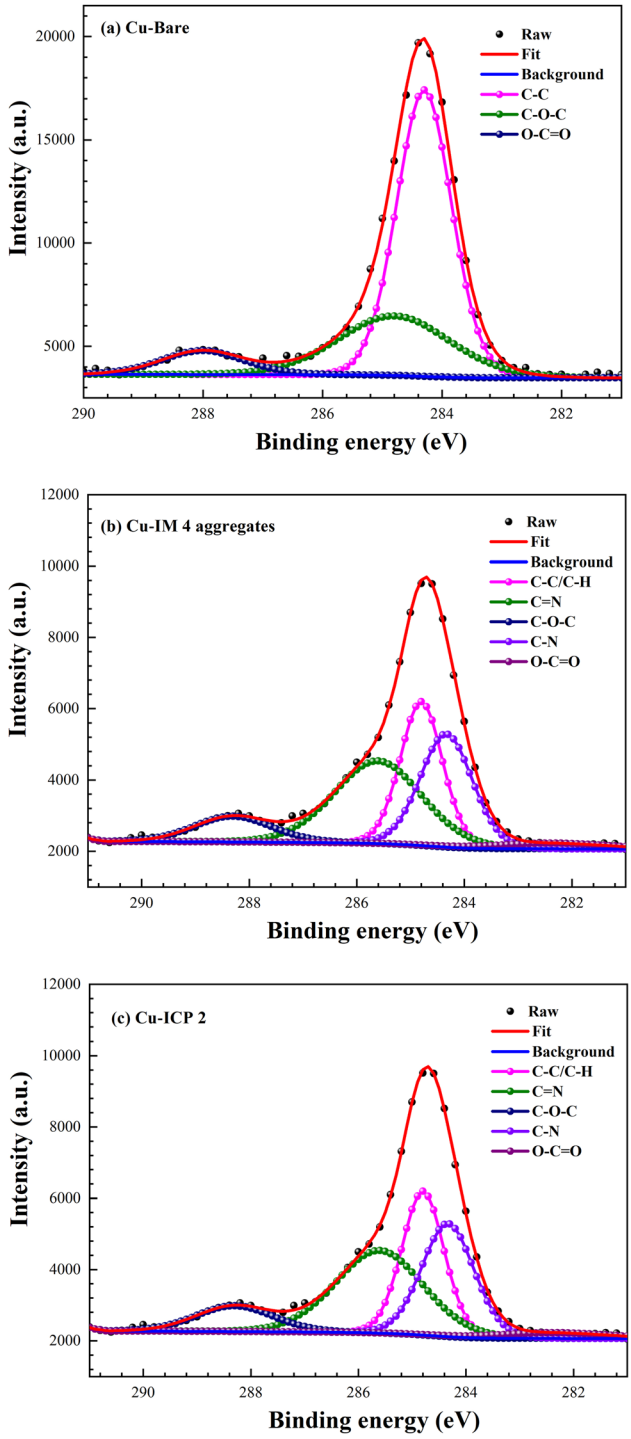

Fig. 8 C 1 s XPS spectra of the studied copper surfaces, (a) the ground bare copper after included in blank 0.5 mol/L sulfuric acid solution, (b-c) the copper surface adsorbed by the stable ICPs after immersion in 0.5 mol/L sulfuric acid solution (the adsorption of ICPs of 0.10 g/L on copper surface: 8 h at 298 K)

plots. The results suggest that the adsorbed ICPs layers prevented from the movement of the dissolved O_2 in the bulk solution to the bulk solution-copper interface, or the migration of the Cu ions from the copper substrate surface into the bulk

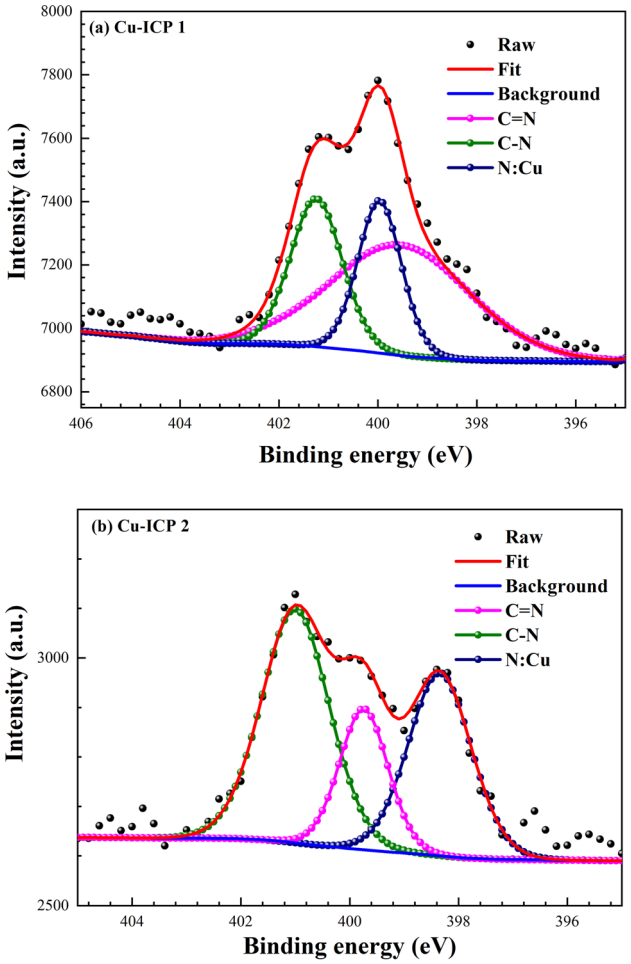

Fig. 9 N 1 s XPS spectra of the studied copper surfaces, copper surface adsorbed by the stable ICPs after immersion in 0.5 mol/L sulfuric acid solution (after the adsorption of ICPs of 0.10 g/L on copper surface: 8 h)

Table 3 De-convolution parameters of N 1 s XPS spectra peaks obtained from the bare copper and the copper adsorbed by the ICPs after the immersion in 0.5 M H_2SO_4 solution (the adsorption of ICPs of 0.10 g/L on copper surface: 8 h)

Samples	Chemistry states	Binging energies, eV	FWHMs, eV
Cu-ICP 1	C=N	399.09	2.21
	C-N	399.98	0.98
	N:Cu	401.32	1.46
Cu-ICP 2	C=N	398.34	1.42
	C-N	399.74	1.09
	N:Cu	401	1.52

solution. Therefore, the kinetic prevention of ORR process of Cu electrode as well as the inhibition of Cu electrode dissolution was intensified by the adsorption of the ICPs on copper electrode. As a consequence, the copper corrosion in H_2SO_4 was suppressed by the ICPs adsorption films.

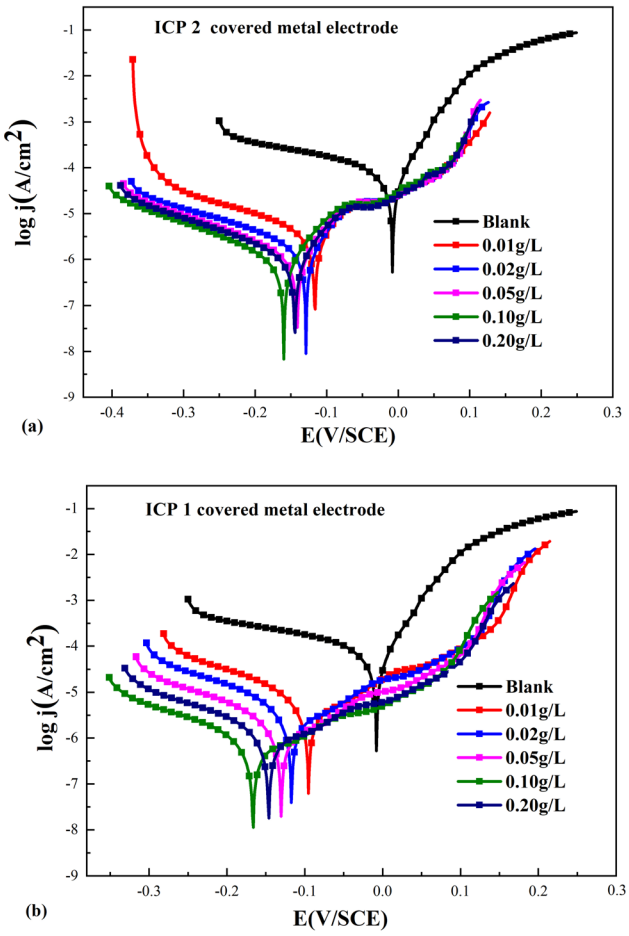

Fig. 10 Tafel curves in 0.5 mol/L H_2SO_4 solution for the blank copper and the copper eletrodes adsorbed by the ICPs of various concentrations at 298 K (the adsorption of ICPs on copper surface: 8 h)

Furthermore, the capacitance arcs in the Nyquist curves of the adsorbed ICPs WEs were enhanced with an increase of the ICPs' concentrations (from 0.01 to 0.10 g/L). On the other hand, the capacitance arc of the ICPs covered WEs showed a decrease as the concentration of the adsorbed ICPs was 0.20 g/L, which suggests that the corrosion inhibition performance of the ICPs could be reduced by the weakened adsorption at 0.20 g/L.

The Bode curves based on the Nyquist plots are further found in Fig. 11 and12. It is shown that the impedance modulus and phase angles of the ICPs adsorbed WEs exhibited an increase with increasing the ICPs' concentrations (from 0.01 to 0.10 g/L), which were reduced at 0.20 g/L. Thus, the peak values were achieved at 0.10 g/L of the ICPs. This shows that the best adsorption of the ICPs on copper surface was gained at 0.10 g/L, and thus the greatest corrosion inhibition effect was achieved.

The electrochemical parameters of EIS plots were obtained by the fitted equivalent circuits (Fig. 13, Table 5). Herein, the CPE_f impedance (Constant phase element) was obtained by the Eq 3 (Ref 47):

$$Z_{CPE} = \frac{1}{Y(j\omega)^n} \quad \text{(Eq 3)}$$

Table 4 Polarization parameters in 0.5 M sulfuric acid solution for the bare copper electrodeand the copper electrodes covered by the ICPs of various concentrations after the immersion in 0.5 M H_2SO_4 solution at 298 K (the adsorption of ICPs on copper surface: 8 h)

Copper electrodes	Polarization parameters					
	c, g/L	E_{corr}, V/SCE	j_{corr}, μA/cm^2	β_c, mV/dec	β_a, mV/dec	η_p, %
Blank	…	− 0.061	64.56	− 275.18	52.87	…
Covered by the ICP 1	0.01	− 0.095	9.617	− 224.27	101.09	85.10
	0.02	− 0.117	5.434	− 179.86	140.67	91.58
	0.05	− 0.130	2.876	− 169.12	97.47	95.55
	0.10	− 0.166	1.716	− 150.67	128.92	97.34
	0.20	− 0.146	3.550	− 177.65	109.18	94.34
Covered by the ICP 2	0.01	− 0.116	8.662	− 202.39	225.23	86.58
	0.02	− 0.129	5.505	− 187.72	502.51	91.47
	0.05	− 0.141	3.421	− 169.29	359.71	94.70
	0.10	− 0.160	1.225	− 172.53	429.55	98.10
	0.20	− 0.144	2.024	− 162.81	228.05	96.59

herein, Y was the admittance of the electrochemical system, j showed the imaginary root, ω was the angular frequency, n represented the deviation parameter ascribed to phase shift. While n was zero, CPE meant a pure resistor, and as n was one, it showed a pure capacitor.

Besides, the C_{dl} and C_f could be computed by the Eq 4 (Ref 48):

$$C_{dl} = Y_0(\omega)^{n-1} = Y_0(2\pi f_{z_{im-Max}})^{n-1} \quad \text{(Eq 4)}$$

herein, $f_{z_{im-Max}}$ showed the frequency at the peak imaginary part in the determined Nyquist plot.

The data indicate that the inhibition of charge transfer and the suppression of polarization of the WEs were strengthened by the adsorbed ICPs films (Table 5). So, the CPE_f and CPE_{dl} showed a decrease. The results suggest that the ICPs adsorption could lead to a substitution of water molecules and aggressive species covered on copper surface, so thus the exposure of the WEs to the attacking acid solution was lowered. Hence, the thickness of electric double-layer was increased, but the local dielectric constant was decreased. As a result, the copper electrode corrosion in H_2SO_4 solution was inhibited by the ICPs adsorption layers.

In addition, the results show that the charge transfer was inhibited more significantly with an increase of the ICPs' concentrations (from 0.01 to 0.10 g/L, Table 5). Therefore, the maximal corrosion inhibition efficiency was reached at 0.10 g/L (ICP1, 98.36, ICP2, 98.53%). It is necessary to point out that the target ICPs carrying iodide or dihydrogen phosphate anions show the better corrosion inhibition effects to copper in H_2SO_4 solution than the intermediate ICP including counter bromide anions (such as at 0.10 g/L, 96.8%) (Ref 49), which could be ascribed to the stronger adsorption of the target ICPs on copper surface. In particular, the η_j of the ICP2 was 97.19% at 0.01 g/L. The EIS results demonstrate that the adsorbed ICPs films showed an excellent anticorrosion performance of copper in acid solution.

3.4 A proposed Adsorption of the ICPs on Copper Surface for Anticorrosion

It is shown that the ICPs adsorption on copper surface might occur through mixed chemical and non-chemical effects. The adsorption of the ICPs on copper surface was performed in EtOH or MeOH/H_2SO_4 (0.01 mM solution) solvents (v/v, 50/50). Hence, the non-chemical effect could be processed as the followings. It is noted that the ICPs are composed of cations and anions. As copper ions were produced and attached to the bulk copper surface, the ICPs could be attached to copper surface through the electrostatic role and van der Waals force.

However, such a process is shown the dependence on free copper ions. It is known that the rapid chemistry coordination between the ICPs and copper ions might yield Cu(I)-ICPs bonding, thus free copper ions could be reduced. Therefore, the electrostatic effect between the ICPs and copper surface could be lowered. This in turn suggests that the adsorption films of the ICPs could be mainly composed by the hydrophobic Cu(I)-ICPs complexes (might be tetradentate coordination, Figure S6 in Supplementary materials). Then, few free ICPs could be further covered outside ICPs-Cu complex films through non-chemical effects including electrostatic effect, π-π interactions as well as van der Waals force. This might guarantee the growth of the adsorption films.

It is found that the contacting angles of adsorption films on copper surface were much lower than 90° (Figure S7 in Supplementary materials). (indicating that the outer adsorption films could be formed by the hydrophilic ICPs, While after the corrosion in H_2SO_4 solution for 8 h, the contacting angles of adsorption films on copper surface were larger than 90° (Figure S8 in Supplementary materials), which suggests that the inner adsorption films might be yielded by the hydrophobic Cu-ICPs complexes). A possible adsorption schematic diagram is given in Fig. 14. Hence, the yielded adsorption layers of the ICPs are composed of the outer less free ICPs films plus the inner more Cu-ICPs complexes films (Fig. 14).

It is accepted that the anodic of copper electrode in H_2SO_4 medium is processed as the equations $Cu \rightarrow Cu^+ + e^-$ and

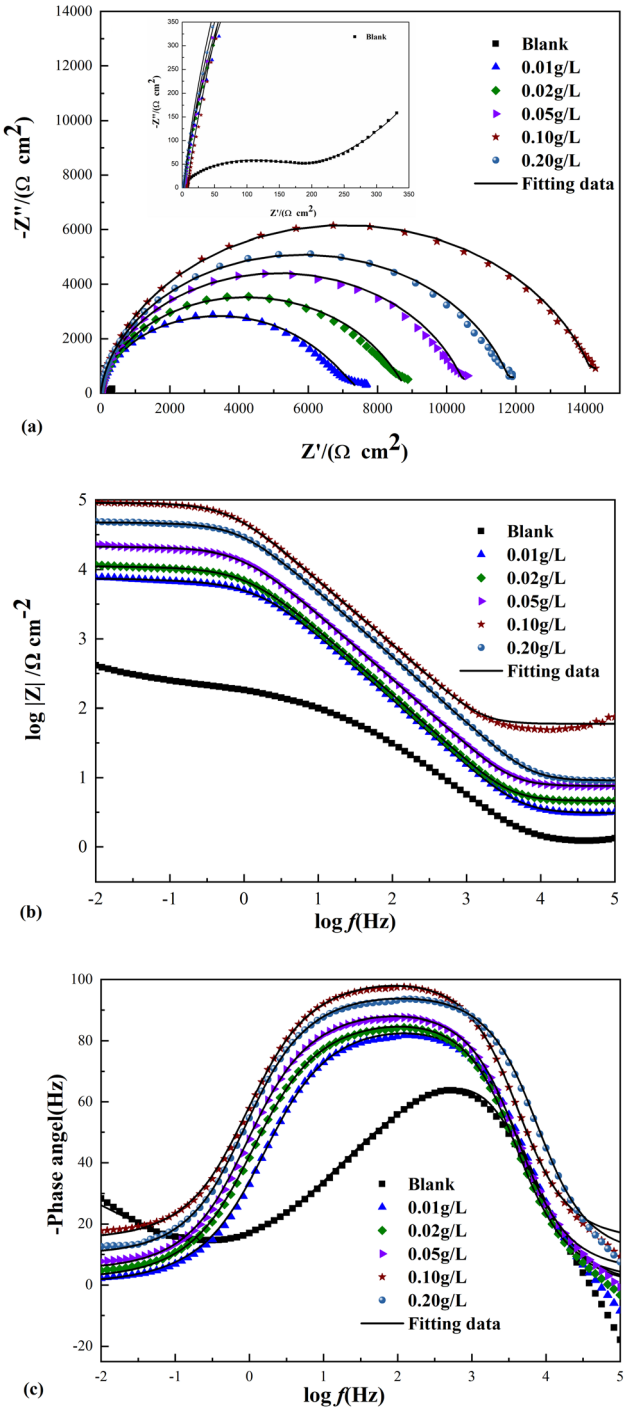

Fig. 11 Plots of (a) Nyquist and Bode (b, c) to the the blank WE and the WEs adsorbed by the ICP2 of differenct concentrations in 0.5 mol/L H_2SO_4 solution at 298 K

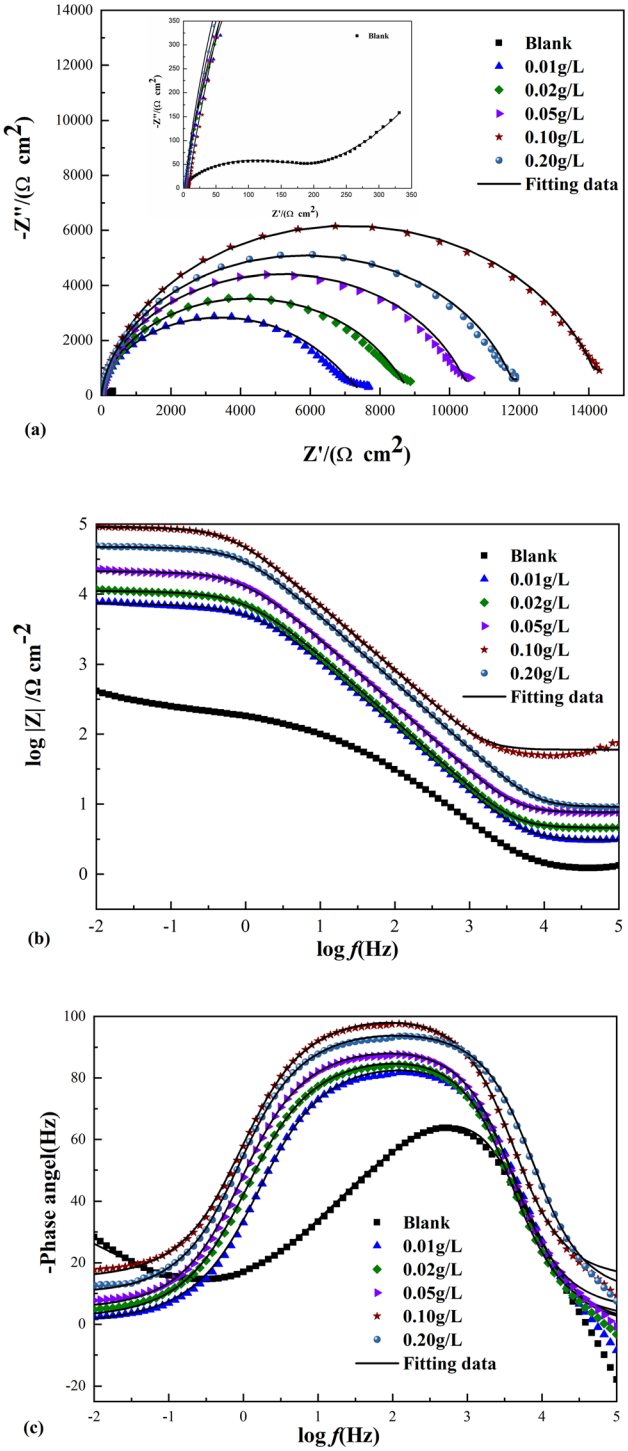

Fig. 12 Plots of (a) Nyquist and Bode (b, c) to the the blank WE and the WEs adsorbed by the ICP1 of differenct concentrations in 0.5 mol/L H_2SO_4 solution at 298 K

$Cu^{+} \rightarrow Cu^{2+} + e^{-}$ (Ref 11, 52, 53). While ORR (oxygen reduction reaction, electrons gaining) in the cathode branch of copper electrode is underwent as $O_2 + 4H^{+} + 4e^{-} \rightarrow 2H_2O$ (Ref 6). Hence, the adsorption films of the ICPs on copper surface could prevent from the diffusion of dissolved oxygen as well as the movement of free charges on the interface between copper surface and the bulk acid solution. In addition, the ICPs adsorption films might inhibit the oxidation of copper in acid solution. Thus, the anodic branch and the cathodic branch of copper electrodes in acid electrolyte could be restrained, and the corrosion inhibition could be more dramatic in the cathodic branch. As a consequence, the ICPs

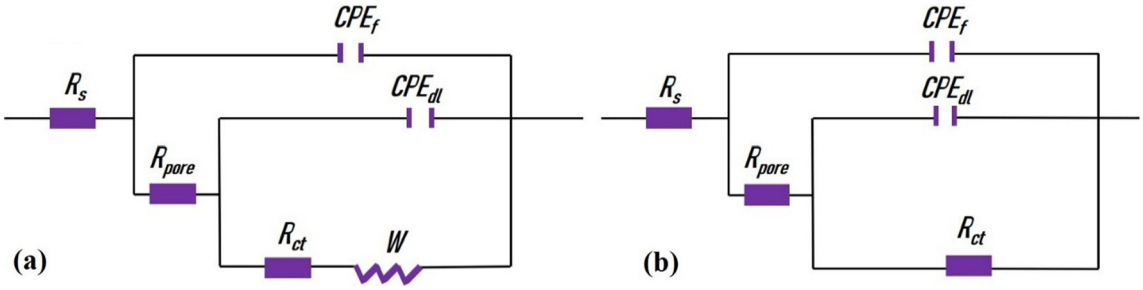

Fig. 13 Equivalent circuits for EIS plots, (a) blank WE; (b) WEs adsorbed by the ICPs; wherein R_s showed the resistance of the solution between WE and RE, R_{ct} were the resistance of the charge transfer, R_f represented the resistance of the pore solution, and W was the Warburg impedance. Besides, the CPE_f (Constant phase element) was composed of C_f (Membrane capacitance) and n_1 (Deviation parameter), and CPE_{dl} *included* C_{dl} (Double-layer capacitance) and n_2 (Deviation parameter)

Table 5 Electrochemical impedance parameters in 0.5 M sulfuric acid solution for the bare copper electrode and the copper electrodes covered by the ICPs of various concentrations after immersion in 0.5 M H_2SO_4 solution (the adsorption of ICPs on copper surface: 8 h)

		Impedance parameters									
Copper electrodes	***C*, g/L**	***R*$_s$, Ω·cm^2**	***R*$_f$, Ω·cm^2**	***R*$_{ct}$, kΩ·cm^2**	***CPE*$_f$, μF/cm^2**	***n*$_1$**	***CPE*$_{dl}$, μF/cm^2**	***n*$_2$**	***W*, μΩ/cm^2**	**η_E, %**	**χ^2, 10^{-4}**
Blank		1.295	7.94	0.20	25.27	1	133.65	0.5503	15390	…	53.5
Covered by the ICP 1	0.01	3.851	164.7	2.604	11.41	0.91	29.20	0.6841	3048	92.24	9.16
	0.02	4.107	217.3	3.219	21.92	0.91	41.87	0.7412	2784	93.72	13.2
	0.05	3.488	252.4	4.962	12.80	0.92	22.44	0.5620	1995	95.93	2.56
	0.10	3.167	367.1	11.73	9.13	0.95	13.60	0.4318	…	98.36	4.10
	0.20	5.983	109.4	7.50	19.44	0.78	65.64	0.5466	…	97.31	10.7
Covered by the ICP 2	0.01	3.314	62.54	7.186	11.35	1	8.96	0.7026	…	97.19	20.2
	0.02	3.681	84.89	8.708	11.09	1	8.38	0.6956	…	97.68	8.73
	0.05	3.807	134.6	10.43	10.65	1	7.57	0.7228	…	98.06	10.5
	0.10	9.499	621	13.74	9.723	1	7.42	0.7591	…	98.53	35
	0.20	2.296	85.45	11.84	9.889	1	6.89	0.7542	…	98.29	6.13

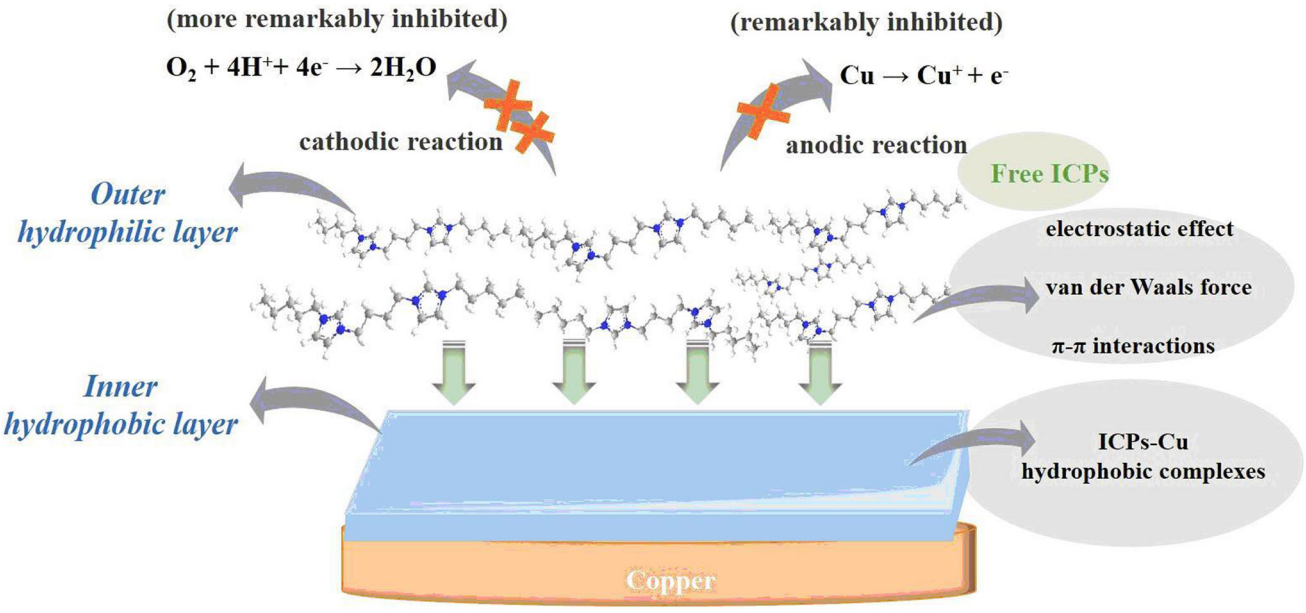

Fig. 14 Possible adsorption schematic diagrams of the ICPs on copper for anticorrosion in H_2SO_4 solution

adsorption films displayed super anticorrosion effect on copper in H_2SO_4 medium

4. Conclusions

This study presented ionic copolymers including iodide and dihydrogen phosphate anions for increased adsorption and anticorrosion on copper in sulfuric acid. The main conclusions were obtained in this study.

1. The ATR-IR, Raman, XPS and XRD demonstrate that the ionic copolymers (ICPs) could form the enhanced adsorption films on copper surface, and the ICPs-copper complexing could be the main driving force for the adsorption.
2. The electrochemistry analysis shows that the copper electrodes could be efficiently protected by the adsorption films of the ICPs. The maximal corrosion inhibition efficiencies of the ICP1 and ICP2 in sulfuric acid for copper were 97.34, and 98.10% at 298 K based on the polarization curves, respectively.
3. The anode and cathode processes of copper electrodes were prevented by the ICPs adsorption films in sulfuric acid. Furthermore, the inhibition of the cathode reaction of copper electrode was more remarkable in H_2SO_4 solution. The results showed that the ICPs could have the strong application potentials for highly efficient anticorrosion of copper in acid medium.
3. This study could guide us to develop new ionic polymers for the achieving the strengthened adsorption and corrosion resistance on copper in acid solutions.

Acknowledgments

We greatly appreciate warm supporting from the National Natural Science Foundation of China (#: 21376282, 21676035 & 21878029). We also appreciate Chongqing Science and Technology Commission (# 2022NSCQ-MSX1298). Y.-T S. thanks the Graduate Student Research Innovation Project, Chongqing University (CYB18046). The authors thank help from the Analytical and Testing Center of Chongqing University.

Conflict of interest

The authors declare no interest conflicts

References

1. M. Mousavi and T. Baghgoli, Application of Interaction Energy in Quantitative Structure Inhibition Relationship Study of Some Benzenethiol Derivatives on Copper Corrosion, *Corros. Sci.*, 2016, **105**, p 170–176.
2. Z. Wang, Y. Gong, L. Zhang, C. Jing, F. Gao, S. Zhang, and H. Li, Self-assembly of New Dendrimers Basing on Strong π-π Intermolecular Interaction for Application to Protect Copper, *Chem. Eng. J.*, 2018, **342**, p 238–250.
3. G. Žerjav and I. Milošev, Protection of Copper Against Corrosion in Simulated Urban Rain by the Combined Action of Benzotriazole, 2-Mercaptobenzimidazole and Stearic Acid, *Corros. Sci.*, 2015, **98**, p 180–191.
4. M.A. Hegazy, A.A. Nazeer, and K. Shalabi, Electrochemical Studies on the Inhibition Behavior of Copper Corrosion in Pickling Acid Using Quaternary Ammonium Salts, *J. Mol. Liq.*, 2015, **209**, p 419–427.
5. A. Yurt and G.Z. Bereket, Combined Electrochemical and Quantum Chemical Study of Some Diamine Derivatives as Corrosion Inhibitors for Copper, *Ind. Eng. Chem. Res.*, 2011, **50**(13), p 8073–8079.
6. B. Duran and G. Bereket, Cyclic Voltammetric Synthesis of Poly(N-Methyl Pyrrole) on Copper and Effects of Polymerization Parameters on Corrosion Performance, *Ind. Eng. Chem. Res.*, 2012, **51**(14), p 5246–5255.
7. M. Bozorg, T. Shahrabi Farahani, J. Neshati, Z. Chaghazardi, and G. Mohammadi Ziarani, Myrtus Communis as Green Inhibitor of Copper Corrosion in Sulfuric Acid, *Ind. Eng. Chem. Res.*, 2014, **53**(11), p 4295–4303.
8. R. Solmaz, E. Altunbaş Şahin, A. Döner, and G. Kardaş, The Investigation of Synergistic Inhibition Effect of Rhodanine and Iodide Ion on the Corrosion of Copper in Sulphuric Acid Solution, *Corros. Sci.*, 2011, **53**(10), p 3231–3240.
9. E.S.M. Sherif and A.H. Ahmed, Synthesizing New Hydrazone Derivatives and Studying Their Effects on the Inhibition of Copper Corrosion in Sodium Chloride Solutions, *Synth. React. Inorg. Met. Org. Nano-Met. Chem.*, 2010, **40**(6), p 365–372.
10. S. Ullah, Study on effect of benzotriazole and Surfactants on Corrosion Inhibition of Copper Alloys in Sulphuric Acid, *Int. J. Electrochem. Sci.*, 2015, **10**, p 8321–8333.
11. B. Tan, S. Zhang, Y. Qiang, L. Guo, L. Feng, C. Liao, Y. Xu, and S.A. Chen, Combined Experimental and Theoretical Study of the Inhibition Effect of Three Disulfide-Based Flavouring Agents for Copper Corrosion in 0.5 M Sulfuric Acid, *J. Colloid Interface Sci.*, 2018, **526**, p 268–280.
12. G.L.F. Mendonça, S.N. Costa, V.N. Freire, P.N.S. Casciano, A.N. Correia, and P.D. Lima-Neto, Understanding the Corrosion Inhibition of Carbon Steel and Copper in Sulphuric Acid Medium by Amino Acids Using Electrochemical Techniques Allied to Molecular Modelling Methods, *Corros. Sci.*, 2017, **115**, p 41–55.
13. S. Zor, M. Saracoglu, F. Kandemirli, and T. Arslan, Inhibition effects of amides on the corrosion of copper in 10 M HCl: theoretical and experimental studies, *Corros. J. Sci. Eng.*, 2011, **67**(12), p 125003.
14. A. Zarrouk, B. Hammouti, A. Dafali, and F. Bentiss, Inhibitive Properties and Adsorption of Purpald as a Corrosion Inhibitor for Copper in Nitric Acid Medium, *Ind. Eng. Chem. Res.*, 2013, **52**(7), p 2560–2568.
15. H. Gerengi, M. Mielniczek, G. Gece, and M.M. Solomon, Experimental and Quantum Chemical Evaluation of 8-Hydroxyquinoline as a Corrosion Inhibitor for Copper in 0.1 M HCl, *Ind. Eng. Chem. Res.*, 2016, **55**(36), p 9614–9624.
16. L. Guo, I.B. Obot, X. Zheng, X. Shen, Y. Qiang, S. Kaya, and C. Kaya, Theoretical Insight Into an Empirical Rule About Organic Corrosion Inhibitors Containing Nitrogen, Oxygen, *And Sulfur Atoms. Appl. Surf. Sci.*, 2017, **406**, p 301–306.
17. Y. Qiang, S. Fu, S. Zhang, S. Chen, and X. Zou, Designing and Fabricating of Single And Double Alkyl-Chain Indazole Derivatives Self-Assembled Monolayer for Corrosion Inhibition of Copper, *Corros. Sci.*, 2018, **140**, p 111–121.
18. R. Fuchs-Godec, and G. Zerjav, Corrosion Resistance of High-Level-Hydrophobic Layers in Combination With Vitamin E-(α-tocopherol) as Green Inhibitor, *Corros. Sci.*, 2015, **97**, p 7–16.
19. E. Kamali Ardakani, E. Kowsari, and A. Ehsani, Imidazolium-Derived Polymeric Ionic Liquid as a Green Inhibitor for Corrosion Inhibition Of Mild Steel in 1.0 M HCl: Experimental and Computational Study, *Colloids Surf.*, 2020, **586**, p 124195.
20. J. Cai, J. Liu, S. Mu, J. Liu, J. Hong, X. Zhou, Q. Ma, and L. Shi, Corrosion Inhibition Effect of Three Imidazolium Ionic Liquids on Carbon Steel in Chloride Contaminated Environment, *Int. J. Electrochem. Sci.*, 2020, **15**, p 1287–1301.
21. W. Luo, S. Zhang, X. Wang, F. Gao, and H. Li, Ionic Macromolecules Based on Non-Halide Counter Anions for Super Prevention of Copper Corrosion, *J. Mol. Liq.*, 2022, **349**, p 118156.
22. Y. Qiang, S. Zhang, L. Guo, X. Zheng, B. Xiang, and S. Chen, Experimental and Theoretical Studies of Four Allyl Imidazolium-Based Ionic Liquids as Green Inhibitors for Copper Corrosion in Sulfuric Acid, *Corros. Sci.*, 2017, **119**, p 68–78.
23. G. Vastag, A. Shaban, M. Vraneš, A. Tot, S. Belić, and S. Gadžurić, Influence of the N-3 Alkyl Chain Length on Improving Inhibition

Properties of Imidazolium-Based Ionic Liquids on Copper Corrosion, *J. Mol. Liq.*, 2018, **264**, p 526–533.
24. R. Hagiwara and Y. Ito, Room Temperature Ionic Liquids of Alkylimidazolium Cations and Fluoroanions, *J. Fluor. Chem.*, 2000, **105**, p 221–227.
25. Y. Shi, Y. Fu, S. Xu, H. Huang, S. Zhang, Z. Wang, W. Li, H. Li, and F. Gao, Strengthened Adsorption and Corrosion Inhibition of New Single Imidazole-Type Ionic Liquid Molecules to Copper Surface in Sulfuric Acid Solution by Molecular Aggregation, *J. Mol. Liq.*, 2021, **338**, p 116675.
26. H. Huang, Y. Fu, F. Li, Z. Wang, S. Zhang, X. Wang, Z. Wang, H. Li, and F. Gao, Orderly Self-Assembly of New Ionic Copolymers for Efficiently Protecting Copper In Aggressive Sulfuric Acid Solution, *Chem. Eng. J.*, 2020, **384**, p 123293.
27. S. Pareek, D. Jain, S. Hussain, A. Biswas, R. Shrivastava, S.K. Parida, H.K. Kisan, H. Lgaz, I.M. Chung, and D. Behera, Improving Enzymatic Hydrolysis of Wheat Straw Using Ionic Liquid 1-Ethyl-3-Methy Limidazolium Diethyl Phosphate Pretreatment, *Bioresour. Technol.*, 2009, **100**, p 3570–3575.
28. D. Fraga, K. Bourahla, M. Rahmouni, J. Bazureau, and J. Hamelin, Catalysed Esterifications in Room Temperature Ionic Liquids with Acidic Counter Anion as Recyclable Reaction Media, *Catal. Commun.*, 2002, **3**(5), p 185–190.
29. M.B.P. Mihajlović, M.B. Radovanović, and ŽZ. Tasić, Imidazole Based Compounds as Copper Corrosion Inhibitors in Seawater, *J. Mol. Liq.*, 2017, **225**, p 127–136.
30. Y. Shi, Y. Fu, H. Huang, H. Li, S. Zhang, W. Li, and F. Gao, New Small Gemini Ionic Liquids for Intensifying Adsorption and Corrosion Resistance of Copper Surface in Sulfuric Acid Solution, *J. Environ. Chem. Eng.*, 2021, **9**, p 106679.
31. S. Pareek, D. Jain, S. Hussain, A. Biswas, R. Shrivastava, S.K. Parida, H.K. Kisan, H. Lgaz, I.M. Chung, and D.A. Behera, New Insight Into Corrosion Inhibition Mechanism of Copper in Aerated 3.5 wt.% NaCl Solution by eco-friendly Imidazopyrimidine Dye: Experimental and Theoretical Approach, *Chem. Eng. J.*, 2019, **358**, p 725–742.
32. S. Qiu, W. Li, W. Zheng, H. Zhao, and L. Wang, Synergistic Effect of Polypyrrole-Intercalated Graphene for Enhanced Corrosion Protection of Aqueous Coating in 3.5% NaCl Solution, *ACS Appl. Mater. Interfaces*, 2017, **9**(39), p 34294–34304.
33. Z. Wang, Y. Tao, Z. Wang, and J. Yan, Synthesis and Characterization of Poly(n-vinyl-1,2,3-Triazole)s Derived from Monomers Obtained by Highly Efficient Wolff's Cyclocondensation, *Polym. Chem.*, 2016, **7**(18), p 3172–3178.
34. P. Song, S. Shen, C.C. Li, X.Y. Guo, Y. Wen, and H.F. Yang, Insight in Layer-by-Layer Assembly of Cysteamine and L-Cysteine on the Copper Surface by Electrochemistry and Raman Spectroscopy, *Appl. Surf. Sci.*, 2015, **328**, p 86–94.
35. S. Ahn, K. Klyukin, R.J. Wakeham, J.A. Rudd, A.R. Lewis, S. Alexander, F. Carla, V. Alexandrov, and E. Andreoli, Poly-Amide Modified Copper Foam Electrodes for Enhanced Electrochemical Reduction of Carbon Dioxide, *ACS Catal.*, 2018, **8**(5), p 4132–4142.
36. Y. Wang, F. Lin, J. Peng, Y. Dong, W. Li, and Y. Huang, A Robust Bilayer Nanofilm Fabricated on Copper Foam for Oil-Water Separation with Improved Performances, *J. Mater. Chem. A*, 2016, **4**(26), p 10294–10303.
37. A. Cánneva, I.S. Giordana, G. Erra, and A. Calvo, Organic Matter Characterization of Shale Rock by x-ray Photoelectron Spectroscopy: Adventitious Carbon Contamination and Radiation Damage, *Energy Fuels*, 2017, **31**(10), p 10414–10419.
38. T. Kosec, D.K. Merl, and I. Milošev, Impedance and xps Study of benzotriazole Films Formed on Copper, Copper-Zinc Alloys and Zinc in Chloride Solution, *Corros. Sci.*, 2008, **50**(7), p 1987–1997.
39. W. Zhou, G. Li, L. Wang, Z. Chen, and Y. Lin, A Facile Method for The Fabrication of a Superhydrophobic Polydopamine-Coated Copper Foam for Oil/Water Separation, *Appl. Surf. Sci.*, 2017, **413**, p 140–148.
40. A. Mezzi, E. Angelini, T. De Caro, S. Grassini, F. Faraldi, C. Riccucci, and G.M. Ingo, Investigation of the Benzotriazole Inhibition Mechanism of Bronze Disease, *Surf. Interface Anal.*, 2012, **44**(8), p 968–971.
41. M. Yann, J. Valentin, T. Nicolas, S.M. Tomo, and H. Jonathan, Iodine Local Environment in High Pressure Borosilicate Glasses: An x-ray Photoelectron Spectroscopy and x-ray Absorption Spectroscopy Investigation, *J. Nucl. Mater.*, 2021, **553**, p 153050.
42. Z. Tao, W. He, S. Wang, and G. Zhou, Electrochemical Study of Cyproconazole as Novel Corrosion Inhibitor for Copper in Acidic Solution, *Ind. Eng. Chem. Res.*, 2013, **52**, p 17891–17899.
43. E.S. Ferreira, C. Giacomelli, F.C. Giacomelli, and A. Spinelli, Evaluation of the Inhibitor Effect of L-Ascorbic Acid on the Corrosion of Mild Steel, *Mater. Chem. Phys.*, 2004, **83**, p 129–134.
44. W. Guo, S. Chen, and M.A. Houyi, A study of the Inhibiton of Copper Corrosion by Triethyl Phosphate and Triphenyl Phosphate Self-Assembled Monolayers, *J. Serb. Chem. Soc.*, 2006, **71**(2), p 167–175.
45. T.T. Qin, J. Li, H.Q. Luo, M. Li, and N.B. Li, Corrosion Inhibition of Copper by 2,5-Dimercapto-1,3,4-Thiadiazole Monolayer in Acidic Solution, *Corros. Sci.*, 2011, **53**(3), p 1072–1078.
46. W. Liu, Q. Xu, J. Han, X. Chen, and Y. Min, A novel Combination Approach for the Preparation of Superhydrophobic Surface on Copper and the Consequent Corrosion Resistance, *Corros. Sci.*, 2016, **110**, p 105–113.
47. Y. Qiang, S. Zhang, S. Yan, X. Zou, and S. Chen, Three Indazole Derivatives as Corrosion Inhibitors of Copper in a Neutral Chloride Solution, *Corros. Sci.*, 2017, **126**, p 295–304.
48. X. Zheng, S. Zhang, W. Li, M. Gong, and L. Yin, Experimental and Theoretical Studies of Two Imidazolium-Based Ionic Liquids as Inhibitors For Mild Steel In Sulfuric Acid Solution, *Corros. Sci.*, 2015, **95**, p 168–179.
49. H. Huang, Y. Fu, X. Wang, Y. Gao, Z. Luo, S. Zhang, H. Li, and L. Chen, Nano- to Micro-Self-Aggregates of New Bisimidazole-Based Copoly(Ionic Liquid)S for Protecting Copper in Aqueous Sulfuric Acid Solution, *ACS Appl. Mater. Interfaces*, 2019, **11**, p 10135–10145.
50. A. Biswas, S. Pal, and G. Udayabhanu, Experimental and Theoretical Studies of Xanthan Gum and its Graft Co-Polymer as Corrosion Inhibitor for Mild Steel in 15% HCl, *Appl. Surf. Sci.*, 2015, **353**, p 173–183.
51. M.M. Solomon and S.A. Umoren, In-situ Preparation, Characterization and Anticorrosion Property of Polypropylene Glycol/Silver Nanoparticles Composite for Mild Steel Corrosion in Acid Solution, *J. Colloid Interface Sci.*, 2016, **462**, p 29–41.
52. H. Huang, Z. Wang, Y. Gong, F. Gao, Z. Luo, S. Zhang, and H. Li, Water Soluble Corrosion Inhibitors for Copper in 3.5 wt% Sodium Chloride Solution, *Corros. Sci.*, 2017, **123**, p 339–350.
53. G.L.F. Mendonça, S.N. Costa, V.N. Freire, P.N.S. Casciano, A.N. Correia, and P.L. Nwto, Understanding the Corrosion Inhibition of Carbon Steel And Copper in Sulphuric Acid Medium by Amino Acids Using Electrochemical Techniques Allied to Molecular Modelling Methods, *Corros. Sci.*, 2017, **115**, p 41–55.